Tellus (1999), 51A, 222–232
Printed in UK – all rights reserved

TELLUS
ISSN 0280–6495

Dynamics, statistics and predictability of a simple limited-area forecasting model

By F. CHOMÉ, S. VANNITSEM and C. NICOLIS*, *Institut Royal Météorologique de Belgique, Avenue Circulaire, 3 – 1180 Bruxelles, Belgium*

(Manuscript received 9 February 1998; in final form 16 October 1998)

ABSTRACT

A canonical model describing the instability of plane wave solutions toward inhomogeneous long wave fluctuations emulating mesoscale atmospheric variability is used to analyze the performance of nested limited-area forecasting models. Comparative studies between a reference fine grid "perfect" model and the ones provided, successively, by a globally coarse and a nested, fine scale, limited-area one are carried out. The statistical properties of the relevant fields are first analyzed, and an optimal size for which the deviations between the "perfect" model and the limited-area one are minimized is identified. Predictability analysis reveals that, although the Lyapunov exponents of the "perfect" model are smaller than those of the globally coarse model, operational error growth proceeds eventually faster in the nested limited-area model than in the globally coarse one.

1. Introduction

During the last years considerable effort has been devoted to the development of fine grid limited-area atmospheric models (LAM) capable of incorporating physical processes affecting weather forecasts (thermal convection, local winds, etc.) that cannot be accounted for properly in traditional coarser global models (Anthes et al., 1987; Gustafsson, 1991).

Ordinarily, a limited-area model is constructed as follows. Within the area of interest a fine grid size discretization scheme is used in integrating the model equations, which takes into account smaller scale phenomena. The boundary conditions necessary are provided at regular times from the integration of a globally coarse model within which the LAM is embedded through appropriate matching techniques at the interface delimiting the fine and coarser grid regions (Juang et al., 1998). Finally, initial conditions are incorporated thanks to the observing network through data assimilation procedures. In state of the art models, the mesh size of the LAM is 10 km or so while the one of the surrounding global coarse model is of the order of 50 km.

At first sight it would seem that the quality of a limited-area model forecast will depend entirely on the physical parameterization schemes added in the model equations, on the way the boundary conditions will be fed and on the quality of the initial data measured at the network stations. Now, as is well known, the atmospheric fields undergo a complex dynamics characterized by the growth of small initial errors as a result of which forecasts become useless beyond a certain time horizon. To complicate matters further, the rate at which these errors grow is far from uniform but depends instead crucially on the atmospheric regime prevailing in a particular region. When assessing the performance of a forecasting model it therefore becomes essential to undertake a detailed

* Corresponding author.
e-mail: cnicolis@oma.be

predictability analysis providing information on the error growth rates and on the regions in which sensitivity is especially pronounced.

Modern predictability analyses are carried out in *phase space*, the space spanned by the full set of the model variables. Owing to the high variability of the local dynamics a statistical viewpoint is adopted. Specifically, several initially close lying trajectories are generated simultaneously and the various properties monitored are averaged over this ensemble or, equivalently, over the invariant probability density on the attractor.

Several authors have reported predictability analyses of operational forecasting models, suggesting an error doubling time of a few days (Simmons et al., 1995). The situation is much less settled for limited-area models. A number of studies (Warner et al., 1997 and references therein) focus on the role of the choice of the boundary conditions in the degradation of the prediction in time. More recently the predictions of regional models have been compared to experimental data and confronted to the results of global models (Ducrocq et al., 1998). In our view these studies are limited by the fact that, for technical reasons, only a few realizations (from one to ten) have been used in performing statistical averages. Furthermore, because of the large number of variables and processes involved it appears difficult to disentangle the origin of the dominant errors responsible for the loss of predictability.

Our objective in the present work is to perform a detailed analysis of a highly simplified limited-area model free of the above limitations. The model chosen describes the instability of plane-wave solutions toward inhomogeneous long wavelength fluctuations known to occur in a number of atmospheric flows, in particular in thermal convection — one of the processes at the basis of mesoscale atmospheric variability (Agee, 1984). It can be shown that near the instability threshold this type of dynamics can be cast in a universal form known as the *complex Landau–Ginzburg equation* (Manneville, 1990; Cross and Hohenberg, 1993). It generates spatio-temporal chaos and therefore exhibits error growth which, as pointed out earlier, is one of the main factors limiting atmospheric predictability.

In Section 2 we present the model and describe the main properties of its solutions. Section 3 is devoted to the design of the regional model. The statistical analysis of the fields generated by the model is presented in Section 4, while Section 5 deals with error growth and predictability of these fields. Finally, we discuss the implications of the main results in Section 6.

2. Model equations

A variety of hydrodynamic flows appear in the form of traveling waves exhibiting a characteristic wave vector q_c and a characteristic frequency ω_c. In systems of large spatial extent the amplitude A of such flows is typically subjected to a modulation on a space and time scale smaller than q_c^{-1} and ω_c^{-1}, reflecting the effect of coupling between the local oscillations. The relevant variable $W(x, t)$ is then given by (we consider for simplicity a 1-dimensional wave pattern)

$$W(x, t) = A(x, t)\, \mathrm{e}^{i(q_c x - \omega_c t)} + \mathrm{cc}, \tag{1}$$

where, cc represents the complex conjugate. Under very general conditions, the amplitude A is shown to obey to a complex equation, known as the complex Landau–Ginzburg equation (Manneville, 1990)

$$\partial_t A = (1 + i\alpha)\partial_x^2 A + \varepsilon A - (1 - i\beta)|A|^2 A. \tag{2}$$

Here, ε is a parameter describing the distance from the bifurcation point at which the traveling wave solutions have been generated, and α, β are real parameters. The cubic term accounts for the saturation of the instability generating the traveling waves by the nonlinearity, whereas the spatial derivative term describes the effects of dissipation and of dispersion through heat, momentum and mass transfer. Hereafter we scale A, x and t in such a way that ε is set equal to unity. Eq. (2) admits then solutions of the form

$$A_0(x, t) = (1 - k^2)^{1/2}\, \mathrm{e}^{i(kx - \Omega_0 t)} \tag{3}$$

with

$$\Omega_0 = -\beta + (\alpha + \beta)k^2. \tag{4}$$

These solutions are stable as long as $\alpha\beta < 1$, $k^2 < (1 - \alpha\beta)[2(1 + \beta^2) + 1 - \alpha\beta]^{-1}$. Beyond this threshold an instability against long-wave modes takes place, referred to as *Benjamin–Feir instability*. Eventually, spatio-temporal chaos sets in, characterized by an erratic dependence of the local phase of the field $A(x, t)$. In the following we will place ourselves in this regime, choosing as parameter values $\alpha = 2.5$, $\beta = -1$ (Shraiman et al., 1994). As analytical techniques are of little use in the chaotic region we resort to a numerical solution of eq. (2) using periodic boundary conditions, emulating in a most natural way systems of large spatial extent. The integration with such boundary conditions is performed using a finite difference numerical scheme of second order in space and time. Specifically, the space derivatives are approximated by centred differences and for the time evolution an implicit Cranck–Nicholson scheme and an Adams–Bashford three level scheme are used, respectively, for the linear and the nonlinear parts (Cattaneo and Hart, 1990). The discretized version of (2) reads

$$A_j^{n+1} = A_j^n + \frac{\Delta t}{2}\left[(\mathscr{L}A^{n+1} + \mathscr{L}A^n) + \left(\frac{23}{6}\mathscr{N}A^n - \frac{16}{6}\mathscr{N}A^{n-1} + \frac{5}{6}\mathscr{N}A^{n-2} \right) \right] \tag{5}$$

with

$$\mathscr{L}A = A + (1 + i\alpha)\frac{\partial^2 A}{\partial x^2},$$

$$\mathscr{N}A = -(1 - i\beta)|A|^2 A$$

where Δt is the time step which is taken to be equal to 0.02 time units.

The spatial power spectrum of the variable $A(x, t)$ is represented in Fig. 1. It is computed from the relation

$$S(k) = \left\langle\!\!\left\langle \left| \frac{1}{N} \sum_{j=1}^{N} A(j)\, e^{i(2\pi/L)kj\Delta x} \right|^2 \right\rangle\!\!\right\rangle \tag{6}$$

where k is the wavenumber, N the number of gridpoints in the interval $L = 400$ space units, Δx the grid size taken to be equal to 1 and $\langle\langle \cdot \rangle\rangle$ represents an ensemble average over 5000 successive (in time) configurations. The continuous character of the spectrum clearly exhibited in Fig. 1, suggests the existence of spatio-temporal chaos for the aforementioned choice of control parameters. To confirm this chaotic behaviour we have computed the Lyapunov spectrum of the system using the algorithm provided by Shimada and Nagashima (1979), with two different grid sizes, $\Delta x = 1$ and $\Delta x = 2$, respectively. The results for the first 100 Lyapunov exponents arranged in decreasing order are shown in Fig. 2. We notice that some of them are positive, thereby corroborating the chaotic nature of the dynamics. The coarse-scale ($\Delta x = 2$ (dots)) and the small-scale ($\Delta x = 1$ (crosses)) systems possess 67 and 48 positive exponents, respectively. Furthermore, the largest exponent for $\Delta x = 1$, $\sigma_{\max}^{(1)} \sim 0.12$ time units^{-1}, is smaller than the one corresponding to $\Delta x = 2$, $\sigma_{\max}^{(2)} \sim 0.16$ time units^{-1}. The above results suggest that the fine grid model is more predictable than the coarse one, in the sense that small initial errors will increase slower. A similar dependence of predictability on the resolution has been observed on a number of atmospheric processes such as the baroclinic jet (Malguzzi et al., 1990), the alpine lee cyclogenesis (Dell'Osso, 1984) or precipitation (Simmons et al., 1989).

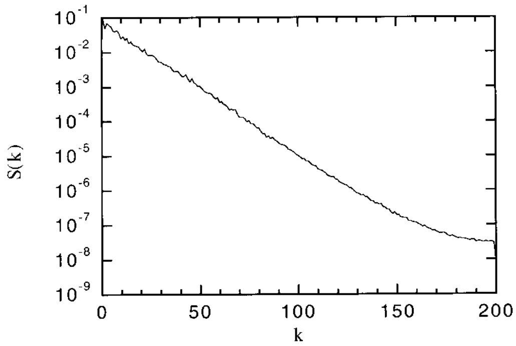

Fig. 1. Spatial power spectrum of the real part of variable A of model (2) with $\Delta x = 1$ space unit, averaged over 5000 time units.

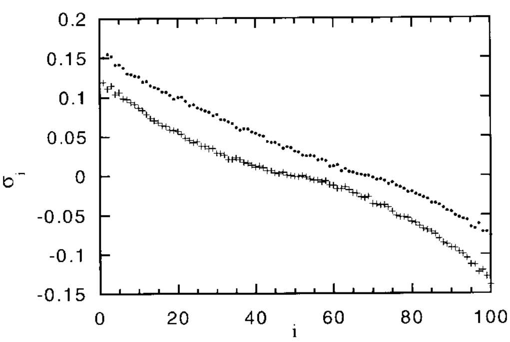

Fig. 2. Spectrum of the 100 dominant Lyapunov exponents of model (2) with $\Delta x = 2$ (dots) and $\Delta x = 1$ (crosses).

On the other hand this result may seem surprising as it is at variance with the experience acquired with realistic full scale numerical weather prediction models, in which higher resolution tends to be associated with larger error growth rates. The explanation of this discrepancy stems from the fact that when a finer mesh is considered in numerical weather prediction models, an improved parameterization of subgrid scale processes is performed and, furthermore, the numerical damping is decreased (Williamson, 1978; Gustafsson, 1996). This has not been the case in our model whose purpose was to assess the role of resolution in the predictability, all other things being equal. Besides, a numerical damping is not needed here thanks to the dissipative character of the model equations. In this respect it is also worth noting that in a recent analysis of a quasi-geostrophic model two of the present authors (Vannitsem and Nicolis, 1997) have shown that the values of the Lyapunov exponents and hence the instability properties of the flow are highly dependent on the choice of the numerical damping.

Finally, it must be emphasized that the type of solutions of eq. (2) depends crucially on the size of the system which plays the role of a privileged bifurcation parameter. In particular, the behaviour depicted in Figs. 1, 2 is observed only when the size exceeds a critical value necessary for the excitation of modes in the appropriate spatial range.

3. The regional model

3.1. *Design of the model*

In this section, we shall emulate the process of nesting a fine grid, limited-area atmospheric prediction model in a coarse grid, global one on our canonical model of Section 2. As stressed already at the end of the preceding section a simplification on the design of our LAM from eq. (2) as compared to realistic models of the atmosphere will be to disregard the problems arising from the adaptation of the parameterization schemes of subgrid processes as the resolution increases. In this respect, therefore, we will limit our study to effects arising solely from the nesting procedure of a limited-area model. Yet despite the simplicity of the setting, the model is still capable of generating complex behaviour sharing key features of atmospheric variability and this will enable us to delineate the role of various factors in the observed behaviour. More importantly, it will allow for a comprehensive analysis of the probabilistic properties since the integrations over a large number of samples starting from different initial conditions can here be carried out at a reasonably low computational cost. This will in turn be a necessary prerequisite for a detailed predictability analysis of the fields of interest generated by the model.

To be concrete, consider a spatial region whose extent is equal to 400 space units, supposed here to represent the entire space in which the dynamics is taking place. We stipulate that "nature" would adequately be described in this space if the model of Section 2 could be integrated with a grid of mesh size $\Delta x = 1$ space unit. But owing to practical limitations, if we are forced to carry out the integration in a "global" scale encompassing the entire system, we can only consider a coarser mesh of $\Delta x = 2$. To come to terms with the need to describe at least some part of the global region (say between nodes 149 and 250) in a more detailed manner we therefore resort to the following "compromise": in the region of interest (the analog of the LAM) the model has the resolution of nature ($\Delta x = 1$), whereas in regions outside this space the information is provided by the globally coarser model. For practical reasons the gridpoints of the global model, however coarse, are taken to be located at the corresponding ones provided by nature. Note that, owing to the difference in the mesh size, the effective spatial couplings in the LAM model and in the outer model are different, even if parameter α in eq. (2) is given the same value in both regions.

To have a well-posed problem one must also prescribe boundary conditions. In both the reference system — the "nature" — and the global model, periodic boundary conditions equating the values of the field and its derivative at the initial and final points will be chosen. As for the limited-area model the boundary conditions necessary for the fine grid integration will be provided at each time step by the globally coarse-grid model in which it is embedded. For this purpose the continuity of the field and its spatial derivative across the interface between the two regions will be required. The above setting emulates the procedure followed in realistic weather prediction LAMs. Note however that in this latter case the boundary condition requirements are somewhat smoothed out through a "coupling" zone surrounding the fine grid model (Gustafsson, 1996).

3.2. *Initialization*

Operational weather forecasting requires the knowledge of the values of atmospheric variables, at some time considered as the "initial state", as provided by the global observational network.

In the context of our formulation the data describing the initial state of the field will be provided by the integration of the reference fine-grid model run over the entire space, which plays here the role of the "nature". The values so obtained will be used as such in the limited-area model, for which the grid size is identical to that of the reference model. In other words, the initial conditions over the LAM area are by construction perfect. To initialize the fields over the coarse-grid space surrounding the region of interest a 3 point linear interpolation scheme will be used. Notice that by adopting this particular initialization scheme we eliminate automatically an important source of error of operational forecasts, in which the data available are collected from a rather sparse set of stations as compared to the points of the above dense grid.

4. Statistical properties of the computed fields

Having initialized the fields one may now integrate the model equations and compare at each time step the difference between the predictions of the limited area-model and the evolution of "nature". As the system operates in the regime of spatio-temporal chaos a direct comparison at the level of a unique realization (phase space trajectory) is not very illuminating, since the results will fluctuate considerably over the successive integration steps. We shall therefore focus on the statistical properties of the field at a particular gridpoint chosen here in the center of the limited-area grid, which by construction is also the center of the fine-scale and global models as well.

In what follows we present the main results for two representative statistical properties : the probability density, P, and the spatial power spectrum. Fig. 3 depicts P of the real part of the variable A at the central point for a LAM of size $L = 180$ space units (dashed lines) and for "nature" (full lines). We observe a symmetry around the mean, which here happens to be at a less probable state (local minimum) of the variable. The two densities are nearly indistinguishable near the mean, but present sizable deviations as one moves to the extremes. As expected, the discrepancy between the P of "nature" of that of the coarse global model (not shown) are much more important. Interestingly, the deviations depicted in Fig. 3 depend on the length, L, of the limited-area model. Fig. 4 describes this dependence using as indicator the mean distance, $|\Delta P|$, measured by recording the deviations of the model from "nature" in all the classes of the histogram (Fig. 3) and averaging over their number. The diagram clearly indicates zones where the mean error is considerably

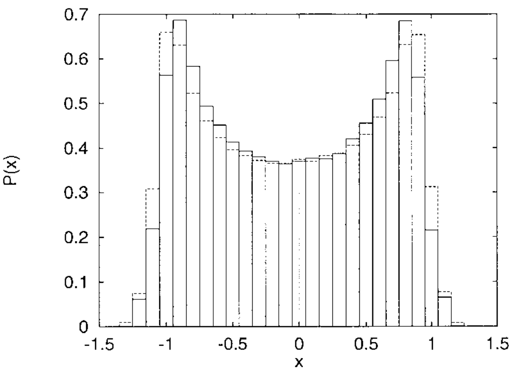

Fig. 3. Probability density P of real(A) of the "nature" model (full line) and of a nested limited-area model of size $L = 180$ space units (dotted line).

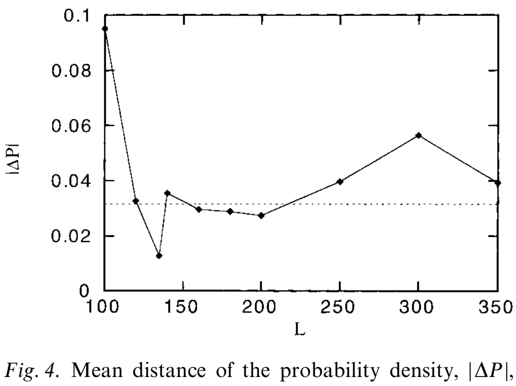

Fig. 4. Mean distance of the probability density, $|\Delta P|$, between the "nature" and the nested limited-area model of length L (full line). The dashed line stands for the deviation between "nature" and a globally coarse model.

reduced. In particular, it allows one to localize a range of size values where one can identify two optimal lengths, $L \sim 133$ and $L \sim 200$ units for which this mean error is practically negligible (less than 3%). The horizontal dashed line represents the deviations of the global coarse model from "nature". It appears therefore that a judicious choice of the length of the nested model may provide statistics of enhanced quality.

We come next to the spatial power spectrum. To arrive at a meaningful comparison we compute, for a given size of the LAM, the spatial power spectrum over the corresponding region and compare it with the one obtained from the perfect model. Fig. 5 depicts a typical result. We observe that for short scales (k large) the agreement is satisfactory but for large scales (k small) the spectrum of the LAM (full line) deviates from "nature" (dashed line) in that it presents a number of equally spaced spurious peaks. As the length of the limited-area model is increased the agreement on short scales subsists. Fig. 6 depicts an error analysis along the lines of Fig. 4 revealing again the existence of an optimal length of about $L = 200$ space units, coinciding with the optimal length of the histogram analysis. This provides one with an additional information on the optimal design of the model.

One might argue that the deviation of the spatial power spectrum from "nature" for long wavelengths is of no major importance since, after all, the main usefulness of a limited-area model is to provide information on the short scales. Still the existence of an optimal length is intriguing,

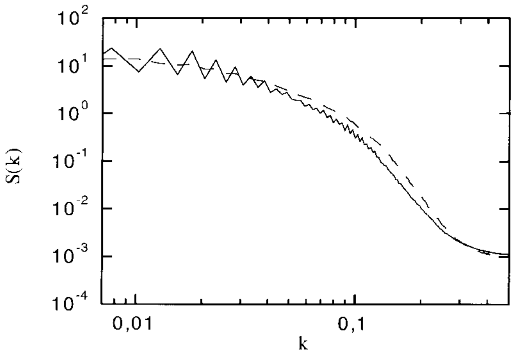

Fig. 5. Spatial power spectrum (normalized to unity) of the "nature" (dashed line) and of a nested limited-area model of size $L = 350$ space units (full line).

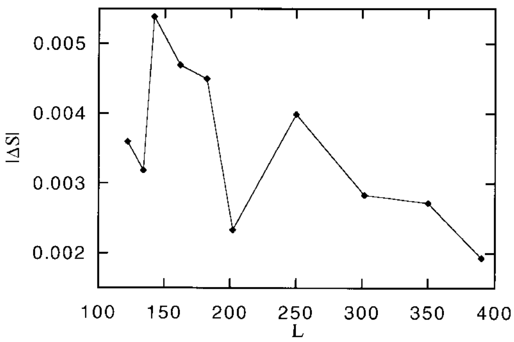

Fig. 6. As in Fig. 4 but for the spatial power spectrum.

since at first sight a larger system should mimic "nature" more closely. We believe that the answer to this apparent paradox lies in the interplay between internal dynamics and the boundary forcing provided on the limited-area model by the coarse, large-scale one in which it is embedded. A small size system mimics nature poorly anyway since it will lack the spatial scales appropriate for the description of phenomena like, e.g., convection for which it was designed. As the size increases more spatial modes become excited (see comments at the end of Section 2) giving rise to a behaviour close to the phenomena one wishes to predict by this type of modelling. Still, for moderate sizes these modes remain fairly distinct. They are therefore not affected substantially by the forcing coming from the boundary conditions. But for still larger sizes the modes representing the various space patterns tend to be distributed in an almost continuous fashion : a minute boundary forcing suffices to mix them up, thereby producing an unrepresentative output.

5. Error growth and predictability

5.1. Formulation

Let $\boldsymbol{x}_0$ be the initial state of the atmosphere, $\boldsymbol{y}_0 = \boldsymbol{x}_0 + \boldsymbol{e}$ a state to which $\boldsymbol{x}_0$ is displaced as a result of an initial error $\boldsymbol{e}$. By definition the instantaneous error E_t is

$$E_t = |\boldsymbol{y}(t; \boldsymbol{y}_0) - \boldsymbol{x}(t; \boldsymbol{x}_0)| \tag{7}$$

where $\boldsymbol{y}(t; \boldsymbol{y}_0)$, $\boldsymbol{x}(t; \boldsymbol{x}_0)$ are obtained by integrating the evolution laws starting at $t = 0$ with the initial conditions $\boldsymbol{y}_0$ and $\boldsymbol{x}_0$, respectively, and $|\cdot|$ is a norm.

Because of the complexity of the dynamics of typical systems of interest in the atmosphere, E_t as defined by eq. (7) fluctuates considerably both over time and over the state space of the system.

To relate the error dynamics in an intrinsic manner to the properties of the underlying system and, more particularly, to the structure of its attractor, we adopt a probabilistic viewpoint. Specifically, the operation defined by eq. (7) is repeated for initial conditions $\boldsymbol{x}_0$ running all over the attractor, and the average error over all these realizations is evaluated,

$$\langle E_t \rangle = \int \mathrm{d}\boldsymbol{x}\, \rho(\boldsymbol{x}_0) |\boldsymbol{y}(t; \boldsymbol{x}_0 + \boldsymbol{e}) - \boldsymbol{x}(t; \boldsymbol{x}_0)| \tag{8}$$

where $\rho(\boldsymbol{x}_0)$ is the invariant probability distribution over the attractor. Additional averaging over $\boldsymbol{e}$ can be performed if necessary.

It is by now established that the time evolution of $\langle E_t \rangle$ follows a universal pattern: a short time regime where errors remain small; an intermediate regime switched on at a time t^* of the order of $t^* \sim \ln(1/|e|)$ where errors become important and vary linearly in time; and a long time regime where mean error reaches a saturation level $\langle E_\infty \rangle$ representative of the structure of the attractor as a whole.

The traditional modelling of this behaviour is based on the idea that the short-time evolution is exponential with a characteristic exponent equal to the system's largest Lyapunov exponent $\sigma_{\max}$. Extensive predictability experiments on highly idealized low-order models (Nicolis and Nicolis, 1993; Vannitsem and Nicolis, 1994) have shown that the situation is actually more involved: owing to the highly inhomogeneous dynamics on the attractor, the rate of mean error growth is variable for short times, starting with a value higher than $\sigma_{\max}$, a behaviour that has been referred to as superexponential (Trevisan, 1993).

In the following we concentrate on the comparison of the predictability properties of the globally coarse and the nested limited-area model, using the fine-grid global model (the "nature") as reference. To this end, we first perturb the fields at each gridpoint by a random error distributed uniformly over all the scales of motion, in order to quantify the sensitivity of the models, viewed as "perfect models", to the uncertainty of the initial conditions. We next perform "operational" error growth experiments whereby, starting from identical initial conditions in the three models at hand, the deviations between trajectories belonging to different attractors, namely, those of the globally coarse model and of the nested limited-area model on the one side, and that of the "nature" on the other side, are computed and compared. The results of these analyses are summarized in Subsections 5.2 and 5.3.

5.2. *Error growth in a "perfect model"*

The mean error growth curves normalized by the initial values as obtained from an averaging over 100 gridpoints (the length of the nested limited-area model) and over 5000 realizations uniformly distributed over the attractors of the three types of models defined in Section 3 are depicted in Fig. 7. The length of the coarse-mesh model is fixed to 400 length units. We observe in all cases an initial stage of decreasing of the error associated, as discussed in detail in Nicolis et al. (1995), with the stabilizing effect of the local negative Lyapunov exponents. This effect is more pronounced in the nested limited-area model, presumably because some of those exponents are active on time scales shorter than those accessible to the global one. Beyond one time unit or so instability takes over and all error curves enter in a growth phase, with essentially identical rates. Still, because of the pronounced initial decrease, the error in the globally coarse model remains

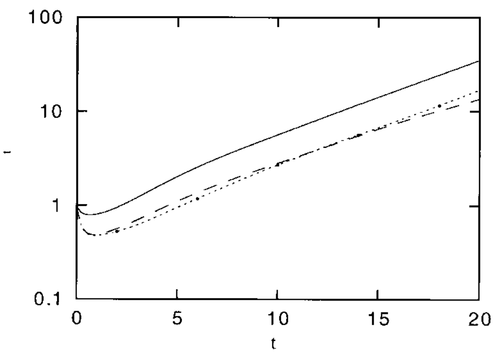

Fig. 7. Mean error evolution, normalized by its initial value, of the globally coarse model (full line), the "nature" (dashed line) and the nested limited-area model (dotted line) as obtained after an averaging over 5000 realizations and over 100 gridpoints (the length of the nested limited-area model).

constantly larger than the one associated to both the limited-area and the "nature" models.

The overall agreement between the two latter models is on the other hand excellent, showing that limited-area models may indeed bring substantial improvements of short range forecasts as compared to the predictability limits inferred from a globally coarse model.

5.3. *Error growth in an imperfect model*

We next focus on operational error growth. Specifically, instead of measuring errors between two slightly different initial conditions evolving in time on a given model, we initialize the limited-area and globally coarse models with "nature", thereby eliminating any source of error associated to the uncertainty of initial conditions. We then let these systems evolve in time and monitor at each time step the difference between the fields of "nature" and those pertaining to the limited-area or the globally coarse model at a given gridpoint. Indeed, owing to the different resolutions and total length of each model, means over the entire domain are not significant since each setting possesses a different attractor.

Notice that the initialization process of the globally coarse model involves interpolation as discussed already in Section 3. The model errors are thus due to the coarseness of the description and to the interpolation of the initial fields as provided by "nature" over the coarse grid. On the other hand, the LAM errors are uniquely due to the nesting procedure through the boundary conditions imposed at the interface.

Fig. 8a depicts how the mean operational error growth at the central gridpoint of the globally coarse (full line) and limited-area nested (dashed line) models evolve, as obtained from an averaging over 5000 realizations and a limited-area size of 200 space units. Note that in order to compare integrations performed with the globally coarse model and "nature", we interpolate at each time step the latter field on the grid of the coarse model. Surprisingly, the error associated to the LAM is larger (Fig. 8b). Fig. 9 (full and dashed lines) shows the same experiment now computed with an initially perturbed state accounting also for the uncertainty in the initial conditions taken to be of the same magnitude in both regions. As in Subsection 5.2 the mean error decreases for short

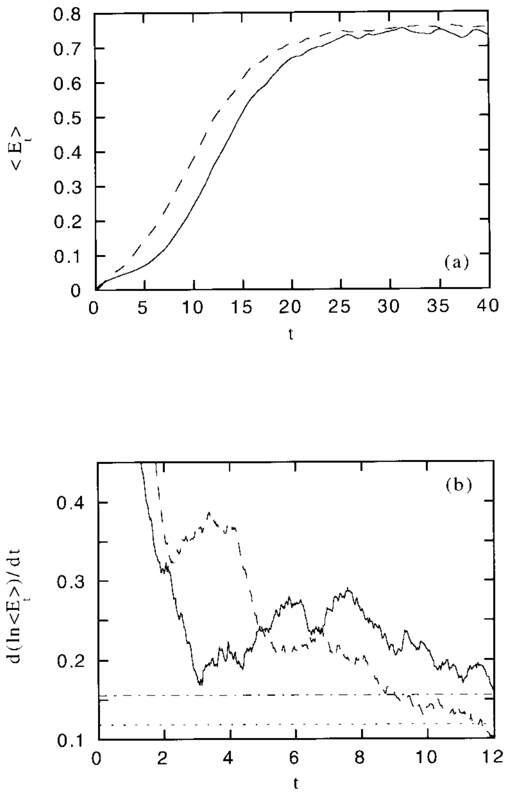

Fig. 8. Performance of the globally coarse model (full line) and the nested limited-area one of size $L = 200$ space units (dashed line) at the central gridpoint, averaged over 5000 realizations. (a) Mean error; (b) mean error growth rate. In both cases initial conditions are those provided by the perfect model ("nature"). Dotted and dotted-dashed lines in (b) represent the maximum Lyapunov exponents of "nature" and the globally coarse model, respectively.

times in both cases and subsequently grows with a rate of 0.21 and 0.25 time units^{-1} for the globally coarse and limited-area models, respectively. Comparing the above curves one realizes that the globally coarse model shows again for all times, a smaller error compared to the regional one in spite of a more pronounced initial decrease of this latter (Fig. 9, bottom right). The dotted line of Fig. 9 reports on the more realistic situation in which the initial errors in the LAM region are half the size of those in the surrounding area. One observes here that during the first 8 time units the mean error curve tends to be lower than the one associated to the global model although the rate

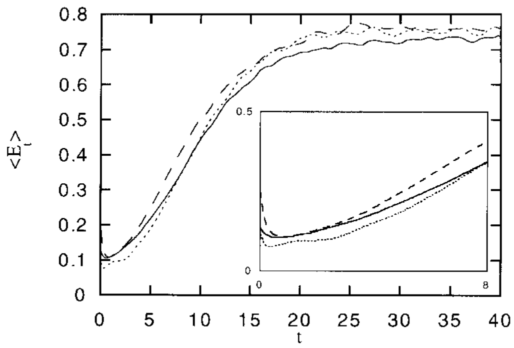

Fig. 9. As in Fig. 8a but initial perturbations uniformly distributed are added over the entire system. Dashed line: the perturbations are of the same magnitude in the LAM and global models. Dotted line: the perturbations in the LAM are half the ones of the global model.

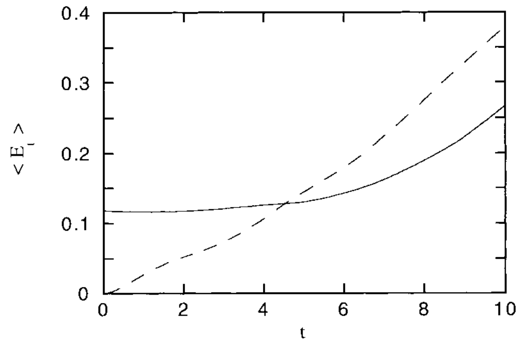

Fig. 10. Mean error evolution for the globally coarse model (full line) to predict phenomena at the scale of LAM (by linear interpolation of two adjacent gridpoints) and of the LAM with $L=200$ space units (dashed line) as obtained from 10000 realizations.

of growth attains a value even larger than in the preceding experiment (0.32 time units^{-1}). Notice that the error dependence on the particular grid chosen is rather weak. The above behaviour is therefore typical of the whole spatial domain.

The explanation for these surprising results resides, undoubtedly, on the combined effect of the dynamics, the limited-area boundary conditions and the interpolation process related to the initialization of the globally coarse model. Despite the absence of initial error in Fig. 8a for the LAM one observes a subsequent error growth at a rate much larger than the one of the globally coarse model during the first 5 units, after which the rates are rather similar until the error reaches saturation. Moreover, these rates are much larger than their corresponding Lyapunov exponents during approximatively 12 time units (see Fig. 8b), suggesting that the mean error does not grow with the commonly accepted exponential law, but much faster. The disrupting effect of the boundary forcing on the limited-area setting accentuates further this trend.

Regarding Fig. 9 part of the explanation is in the fact that the initial error in the nested limited-area model is much larger, owing to the smoothing action of the interpolation process which tends to average out the initial errors in the coarse model. Nevertheless, the decreasing stage of errors in the limited-area model observed for very short times may be of interest for nowcasting and opens the way for possible improvements using an appropriate data assimilation scheme (Fig. 9, dotted line). Globally however, the model errors remain present, dominating largely the errors due to the uncertainty of initial conditions.

The above results seem at first sight to lead to the uncomfortable conclusion that, contrary to common expectation, the forecasting skill of the LAM is lesser than that of the globally coarse one. Now this overlooks the fact that in the coarse model one has no direct access to scales which are present in the LAM. To see how the two models fare on such points we perform a downscaling of the large-scale field, creating by simple interpolation intermediate gridpoints over the globally coarse model. We then compare the latter as well as the LAM with “nature” by computing the mean error growth at one gridpoint not resolved by the coarse-mesh model. The results, summarized in Fig. 10, show that the LAM (with $L=200$ space units) exhibits, for short times, enhanced predictability as compared to the “interpolated global model”. This allows one to characterize more sharply the type and quality of new information brought out by the limited-area model.

6. Discussion

In this paper, the dynamical and statistical aspects of nested limited-area weather forecasting models have been addressed using a simplified model of relevance in mesoscale atmospheric variability. Our main goal was to contribute to the solution of two problems of considerable concern: first whether the description of the fields over the limited-area considered is reasonably close to reality; and second, whether the quality of the forecast itself provided by the nested limited-area model is enhanced as compared to that of a globally coarse one.

Owing to the relative compactness of the model a large number of realizations could be carried out producing systematic statistically meaningful results from which the role of the different factors affecting the observed behaviour could be disentangled.

A first series of quantities analyzed are the probability distribution and the spatial power spectrum of the field generated by the limited-area model in comparison with a "perfect" globally fine-grid model. As it turns out the power spectrum of the LAM displays a spurious oscillation at low wavenumbers. We suggest that these could be at the origin of the bias occurring in operational regional forecasts of temperature and wind direction in the lowest levels of the atmosphere during clear nights (Sandev, 1997). Still, an optimal length has been identified for which the differences between the limited-area and the "perfect" model could be minimized. This result may be of practical interest in realistic NWP models where an optimal size of the limited-area model can also be identified.

As regards predictability, a series of experiments has been carried out comparing the performance of the nested limited-area model and of the globally coarse model, using a "perfect" model as reference. Unexpectedly, it turned out that the growth of model errors was faster in the limited-area than in the global coarse case, despite the fact that the Lyapunov exponents of the globally fine-grid model are smaller than those of the globally coarse one. This behaviour was not modified when adding small initial errors arising from the uncertainty to the initial conditions. Neverthless, it turned out that the LAM tends to reduce initial very short range errors (cf. Fig. 9) suggesting enhanced quality forecasts for very short time scales which, in turn, may improve the quality of atmospheric analyses. Moreover, as could be expected, the quality of the forecast at smaller scales for which only the limited-area model gives a prediction is better than the simple interpolation between the closest gridpoints of the globally coarse model.

As pointed out in Sections 2 and 3 the increase of resolution in the LAM was carried out by keeping all model parameters at fixed values, equal to those of the lower resolution one. One may argue that a change of these parameters reflecting, for instance, the influence of short-scale processes would lead the LAM system to a different regime of spatio-temporal chaos characterized by different error growth rates. It would therefore undoubtedly be interesting to extend the present analysis by modifying some of the parameters of eq. (2) in the LAM in a way to mimic events not accounted for in the outer coarse model.

Our study highlights the extreme complexity of the dynamics of limited-area models. In particular, the influence of model errors in the degradation of the quality of forecast reflects the importance and intricacy of the coupling between the nested fine-grid and the surrounding coarse parts of the model. Recently, an alternative and probably more consistent nesting technique has been considered (Juang et al., 1998). It would be of interest to investigate its performance using the model considered in this study.

Future work in this area should also aim at clarifying further the role of the coupling on the intrinsic properties of the dynamics. In particular, its influence on the spectrum of the Lyapunov exponents, on their local variability and on the properties of the corresponding Lyapunov vectors should be assessed. An effort should also be made to apply our techniques to operational limited-area models, the specific objective being here to characterize more sharply the quality of the model forecasts, at least for some key fields, using the various indicators introduced in the present paper.

7. Acknowledgements

We are indebted to Dr. Z. Toth for his multiple suggestions and to Referee B for the comment concerning the role of the choice of different parameters in the limited area and the global models. This work is supported by the Interuniversity Attraction Poles program of the Belgian Federal Office of Scientific, Technical and Cultural Affairs. F. Chomé is a fellow at the "Fonds pour la formation à la Recherche dans l'Industrie et l'Agriculture".

REFERENCES

Agee, E. M. 1984. Observations from space and thermal convection: a historical perspective. *Bull. Am. Meteorol. Soc.* **65**, 938–949.

Anthes, R. A., E. Y. Hsie and Y.-H. Kuo, 1987. *Description of the Penn State/NCAR Mesoscale model version 4 (MM4).* NCAR Technical Note, NCAR/TN-282+STR, 66 pp. (Available from the National Center for Atmospheric Research, PO Box 3000, Boulder, CO 80307, USA.)

Cattaneo, F. and J. E. Hart, 1990. Multiple states for quasi-geostrophic channel flows. *Geophys. Astrophys. Fluid Dynamics* **54**, 1–33.

Cross, M. C. and P. C. Hohenberg, 1993. Pattern formation outside of equilibrium. Rev. Mod. Phys. **65**, 3, II.

Dell'Osso, L. 1984. High resolution experiments with the ECMWF model. A case study. *Mon. Wea. Rev.* **112**, 1853–1883.

Ducrocq, V., D. Tzanos and S. Senesi 1998. Diagnostic tools using a mesoscale NWP model for the early warning of convection. *Meteorol. Applic.*, in press.

Gustafsson, N. 1991. The HIRLAM model. ECMWF Seminar: *Proc. on Numerical methods in atmospheric models.* Reading, UK, pp. 115–146.

Gustafsson, N. 1996. A comparison of the HIRLAM gridpoint and spectral semi Lagrangian models. *Mon. Wea. Rev.* **124**, 2008–2022.

Juang, H.-M., S.-Y. Hong and M. Kanamitsu, 1998. The NCEP regional spectral model. an update. *Bull. Amer. Met. Soc.* **78**, 2125–2143.

Malguzzi, P., A. Trevisan and A. Speranza, 1990. Statistics and predictability for an intermediate dimensionality model of the baroclinic jet. *Ann. Geophys.* **8**, 29–36.

Manneville, P. 1990. *Dissipative structures and weak turbulence.* Academic Press, San Diego.

Nicolis, C. and G. Nicolis, 1993. Finite time behaviour of small errors in deterministic chaos and Lyapunov exponents. *Bifurcation and Chaos* **3**, 1339–1342.

Nicolis, C., S. Vannitsem and J.-F. Royer, 1995. Short range predictability of the atmosphere and Lyapunov exponents. *Q. J. R. Meteorol. Soc.* **1**21, 705–722.

Sandev, M. 1997. Unrealistic cooling during clear winter nights. *Proc. 3rd RC LACE/ALADIN Workshop on the Use of ALADIN products in forecasting practice and verification matters.* Budapest, Hungary, pp. 83–97.

Shimada, I. and T. Nagashima, 1979. A numerical approach of dissipative dynamical systems. *Prog. Theor. Phys.* **61**, 1605–1616.

Simmons, A. J., D. M. Burridge, M. Jarraud, C. Girard and W. Wergen, 1989. The ECMWF medium-range prediction models. Development of the numerical formulations and the impact of increased resolution. *Meteorol. Atmos. Phys.* **40**, 28–60.

Simmons, A. J., R. Mureau and T. Petroliagis, 1995. Error growth and estimates of predictability from the ECMWF forecasting. *Q. J. R. Meteorol. Soc.* **121**, 1739–1771.

Shraiman, B. I., A. Pumir, W. Van Saarloos, P. C. Hohenberg and H. Chaté, 1994. Spatiotemporal chaos in the one-dimensional complex Ginzburg–Landau equation. *Physica D* **57**, 241–248.

Trevisan, A. 1993. Impact of transient error growth on global average predictability measures. *J. Atmos. Sci.* **50**, 1016–1028.

Vannitsem, S. and C. Nicolis, 1994. Predictability experiments on a simplified thermal convection model: the role of spatial scales. *J. Geophys. Res.* **99**, 10,377–10,385.

Vannitsem, S. and C. Nicolis, 1997. Lyapunov vectors and error growth patterns in a T21L3 quasi-geostrophic model. *J. Atmos. Sci.* **54**, 347–361.

Warner, T. T., R. A. Peterson and R. E. Treadon, 1997. A tutorial on lateral boundary conditions as a basic and potentially serious limitation to regional numerical weather prediction. *Bull. Amer. Met. Soc.* **78**, 2599–2617.

Williamson, D. A. 1978. The relative importance of resolution, accuracy and diffusion in short range forecasts with the NCAR Global Circulation Model. *Mon. Wea. Rev.* **106**, 69–88.